

Active epoxidation bipyridine-oxodiperoxotungstate catalysts

Gabriel Hidalgo, Gabriella Barozzino-Consiglio, Michel Devillers, Eric M. Gaigneaux*

^a Institute of Condensed Matter and Nanosciences (IMCN), Université Catholique de Louvain, Place Louis Pasteur, 1, box L4.01.09, Louvain-la-Neuve 1348, Belgium

ARTICLE INFO

Keywords:

Venturello
Bipyridine
Keggin
Heteropoly compounds
Epoxidation

ABSTRACT

Herein, we report the preparation of four compounds obtained by the reaction of $\text{H}_3\text{PW}_{12}\text{O}_{40}/\text{H}_3\text{PO}_4/\text{H}_2\text{O}_2$ with 2,2'-bpy (**a-22**) or 4,4'-bpy (**a-44**) and $\text{H}_3\text{PW}_{12}\text{O}_{40}/\text{H}_2\text{O}_2$ with 2,2'-bpy (**b-22**) or 4,4'-bpy (**b-44**) for the catalytic epoxidation of cyclooctene with H_2O_2 under monophasic conditions. The anions of the four compounds are composed of oxodiperoxotungstate $\text{WO}(\text{O}_2)_2$ moieties and their overall anionic structures are less condensed than the pristine $[\text{PW}_{12}\text{O}_{40}]^{3-}$ polyoxometalate (PW_{12}) precursor (Raman and IR spectroscopies). The peroxy anions and bipyridine interact in a way differing from one bpy isomer to the other. Isomer 4,4'-bpy interacts electrostatically with the peroxy species and 2,2'-bpy in a coordinative mode. Compounds synthesized with isomer 2,2'-bpy (**a-22** and **b-22**) are more epoxidation-active than those containing 4,4'-bpy (**a-44** and **b-44**). Compounds **a-22** and **b-22** share the same structure (PXRD), but **a-22** exhibits substantially better catalytic activity. This superior catalytic efficiency is associated to the presence of phosphatooxoperoxotungstates PW_n ($n = 1; 2; 3; 4$) species with high n value (namely $\text{PW}_4 > \text{PW}_3 \gg \text{PW}_2$) (^{31}P NMR and Raman spectroscopies). The PW_n species are produced before reaction with bipyridine as a result of the degradation of PW_{12} with H_2O_2 which, under the employed conditions, is complete after 30 min. In the aqueous solution, the PW_n species are present in different concentrations and coexist in a fast-dynamic equilibrium. Under the operated catalytic conditions, our materials outperform the homogeneous benchmark catalyst of Venturello ($(\text{C}_6\text{H}_{13})_4\text{N}^+$) $_3[\text{PW}_4\text{O}_{24}]^{3-}$) which shows poor activity. The most active **a-22** and **b-22** catalysts are partially dissolved in the liquid medium, but they precipitate as the epoxide builds in the reaction medium, allowing for potential catalyst separation and reuse. It is revealed that H_2O_2 is required not only to generate epoxidation activity, but to preserve the structure of the catalyst, since without it, the structural damaged appears irreversible.

Introduction

The undeniable success of polyoxometalates (POMs) in catalytic oxidation reactions, has continuously encouraged research groups to exploit and value their intriguing chemical properties [1]. Many of these efforts have been directed towards the development of meticulous catalytic systems combining H_2O_2 as a green oxidant [2] and POMs, especially those with Keggin $[\text{XM}_{12}\text{O}_{40}]^{n-}$ (where $\text{M}=\text{W}, \text{Mo}$; $\text{X}=\text{P}$) structure to oxidize different organic substrates. Particular attention has been given to tungsten-based Keggin anions that, compared to their molybdenum analogues, have shown to be the most catalytically efficient Keggin subsets in oxidation reactions [3,4]. One relevant example is that of Ishii et al. who, in the mid-1980s, developed a promising biphasic system combining Keggin $\text{H}_3\text{PW}_{12}\text{O}_{40}$ phosphotungstic acid (PTA) and the phase transfer agent cetyl pyridinium chloride [5,6] to selectively epoxidize olefins and allylic alcohols. Independently,

Venturello et al. were able to isolate and solve the molecular structure of the polyperoxotungstate $\{\text{PO}_4[\text{W}(\text{O})(\text{O}_2)_2]_4\}^{3-}$ complex (PW_4) from a tungstate-phosphate association under biphasic conditions [7,8]. The postulated catalytically active peroxy species was later identified as the oxygen transfer agent in the Ishii-system [9]. Further spectroscopic and kinetic evidence revealed that PW_4 was not only the dominant epoxidizing agent, but the most kinetically significant one among other polytungstophosphate species derived from the catalytic oxidation itself, and by the reaction with H_2O_2 [10–12]. Since then, the chemistry of Ishii-Venturello has sparked a substantial amount of scientific research devoted to further optimize these systems. A variety of selective oxidation strategies have been developed combining PW_4 with new quaternary ammonium cations (QACs) possessing phase-transfer properties to work under biphasic conditions [13–19]. Other groups have achieved the heterogenization of PW_4 on a number of different supports [20–25]. Yet, besides QACs, scarce amount of research has been

* Corresponding author.

E-mail address: eric.gaigneaux@uclouvain.be (E.M. Gaigneaux).

<https://doi.org/10.1016/j.mcat.2022.112479>

Received 27 April 2022; Received in revised form 24 June 2022; Accepted 27 June 2022

2468-8231/© 2022 Elsevier B.V. All rights reserved.

conducted to explore new kinds of ligands across the plethora of accessible organic molecules. Alongside this, organonitrogen ligands, such as pyrazine, phenanthroline, terpyridine, and bipyridine, have proven to present structure-directing properties in metal oxide networks [26–29], as well as serve as organic platforms with highly modular hydrophobic and redox properties [30–33]. This ability, coupled with the inherent redox properties offered by the chemistry of Ishii-Venturello, could potentially determine desired physicochemical properties in a controllable and predictable manner. As part of our continuous research on the catalytic and structural role of bipyridine isomers in compounds made of Keggin PTA [34], we report here the study of bipyridine-based catalysts synthesized under Ishii-Venturello conditions. The present study has been undertaken for four reasons. Firstly, no catalytic data, to the best of our knowledge, has yet been proposed for compounds prepared from bipyridine and the Ishii $\text{PW}_{12}\text{O}_{40}^{3-}/\text{H}_2\text{O}_2$ system. Secondly, the catalytic and structural properties of compounds synthesized by combining bipyridine with $\text{PW}_{12}\text{O}_{40}^{3-}/\text{H}_2\text{O}_2$ or $\text{PW}_{12}\text{O}_{40}^{3-}/\text{H}_2\text{O}_2/\text{H}_3\text{PO}_4$ systems, have not been systematically investigated. Thirdly, little attention was given to the study of the effects of ligand isomerism in POM-based catalytic systems. This could potentially serve as a tactic to redirect or control the formation of targeted hybrid compounds, and in turn, provide desired catalytic outcomes. The fourth and primary motivation for this study, is the intriguing challenge of developing new and efficient epoxidizing functional materials with a good level of prediction, understanding their structure/activity relationship, and widening the avenues covered by the Ishii-Venturello chemistry.

Experimental section

Materials

2,2'-Bipyridine (2,2'-bpy) (99 %) and 4,4'-bipyridine (4,4'-bpy) (98%) from TCI chemicals; hydrogen peroxide (H_2O_2 , 30 wt.%) and benzene (C_6H_6 , 99%) from Carl Roth; cyclooctene (C_8H_{14} , 95%), dibutyl ether ($\text{C}_8\text{H}_{18}\text{O}$, 99%, stabilized with BHT) and acetonitrile ($\text{C}_2\text{H}_3\text{N}$, for HPLC, isocratic grade) from VWR chemicals; *ortho*-phosphoric acid (H_3PO_4 , 85%) from Merck; cyclooctene oxide ($\text{C}_8\text{H}_{14}\text{O}$, 99%), tungstic acid (H_2WO_4 , 99%), trimethyl phosphate ($\text{C}_3\text{H}_9\text{O}_4\text{P}$, 99%) and tetrahexylammonium chloride ($\text{C}_{24}\text{H}_{52}\text{ClN}$, 96%) from Sigma Aldrich, were purchased and used as received. PTA was purchased from Sigma Aldrich in the form of $\text{H}_3\text{PW}_{12}\text{O}_{40}\cdot x\text{H}_2\text{O}$ (reagent grade) and later dried under vacuum to obtain its hexahydrate form $\text{H}_3[\text{PW}_{12}\text{O}_{40}]\cdot 6\text{H}_2\text{O}$.

Synthesis

Preparation of compounds a-22 and a-44 (method (a))

$\text{H}_3[\text{PW}_{12}\text{O}_{40}]\cdot 6\text{H}_2\text{O}$ (1 mmol, 2.9881 g) was added to 30 wt% H_2O_2 (100 mmol, 10.21 mL). After reaction for 1 h at room temperature, H_3PO_4 (2 mmol, 134.8 μL) was added. After stirring (500 rpm) for 1 h, the solid ligand 2,2'-bpy (3 mmol, 0.4733 g; **a-22**) or 4,4'-bpy (1.5 mmol, 0.2343 g; **a-44**) was added to the aqueous solution. The resulting suspension was stirred for 1 h and the solid was then separated from the solution by filtration. The collected white particles were rinsed several times with water and dried overnight under vacuum (*ca.* 1.8×10^{-2} mbar) at room temperature.

Preparation of compounds b-22 and b-44 (method (b))

The same protocol as method (a) was followed, but without addition of H_3PO_4 .

Preparation of $\text{Q}_3\{\text{PO}_4[\text{W}(\text{O})(\text{O}_2)_2]_4\}$ (Q^+ = tetrahexylammonium)

The synthesis is achieved according the method described by Venturello et al. [7,8]. Tungstic acid (10 mmol, 0.5237 g) was treated with 30 wt.% hydrogen peroxide (70 mmol, 7 mL). After 60 min reaction at 60 °C, and then filtration, H_3PO_4 (2.5 mmol, 168.6 μL) was added. The

solution was stirred 15 min, and then tetrahexylammonium chloride (4 mmol, 1.6255 g) dissolved in benzene (40 mL) was added dropwise over 2 min. The obtained white precipitate (hereafter noted IV-PW₄) was separated by filtration from the biphasic mixture, which was washed with a small amount of water, benzene, and diethyl ether, and dried overnight under vacuum (*ca.* 1.8×10^{-2} mbar) at room temperature.

Preparation of compounds (2,2'-Hbpy)₃[PW₁₂O₄₀] and (4,4'-H₂bpy)_{1.5}[PW₁₂O₄₀] \cdot 1.5H₂O

To an aqueous mixture of PTA (1 mmol, 2.9881 g) in 9.5 mL of distilled water, was added 2,2'-bpy (3 mmol, 0.4733 g, for (2,2'-Hbpy)₃[PW₁₂O₄₀]) or 4,4'-bpy (1.5 mmol, 0.2343 g, for (4,4'-H₂bpy)_{1.5}[PW₁₂O₄₀] \cdot 1.5H₂O) and stirred (500 rpm) during 1 h at room temperature. The resulting suspension was transferred to a sealed stainless-steel autoclave (70 mL) equipped with a Teflon jacket and heated to 120 °C for 5 h, then cooled to room temperature. The resulting white precipitate was filtered, rinsed several times with distilled water and dried overnight under vacuum (*ca.* 1.8×10^{-2} mbar) at room temperature.

Characterization of samples

Powder X-ray diffraction (PXRD) patterns were recorded at room temperature on a Bruker-D8 advance diffractometer (Bragg-Brentano geometry), equipped with a LYNXEYE XE-T detector, using Cu K α radiation ($\lambda = 0.15418$ nm). The X-ray source was operated with a tension of 40 kV and a current of 30 mA. Diffractograms were collected between 5° and 80° (2 θ) and rotated to 5 rpm with a 0.015° increment and 0.15 s per integration step.

Thermogravimetric analysis–mass spectrometry (TGA-MS) was performed in a Mettler Toledo TGA/DSC 3+ apparatus coupled with a Pfeiffer Vacuum ThermoStar mass spectrometer. The samples were initially stabilized at 25 °C during 15 min, and subsequently heated from 25 °C to 900 °C at 10 °C/min under air flow (50 mL/min, 80% N₂ and 20% O₂ Alphagaz 1 Air Liquide).

The weight percentages of W and P were measured by inductively coupled plasma-atomic emission spectrometry (ICP-AES) on an ICP 6500 Thermo Scientific equipment. The samples were calcined at 500 °C and subsequently decomposed by addition of sodium peroxide.

Fourier transform infrared spectra (FTIR) were recorded in a Bruker Equinox 55 with a DTGS detector equipped with a Bruker ATR platinum cell with diamond crystal. The spectra were obtained by recording 500 scans from 400 to 4000 cm^{-1} with 4 cm^{-1} resolution in transmittance mode.

Raman spectra for solid samples were recorded on a Bruker spectrometer (type RFS100/S) equipped with a liquid nitrogen detector and a Nd:YAG laser supplying the excitation line at 1064 nm with a power of 100 mW. The spectra were collected recording 32 scans in the range of 400–4000 cm^{-1} at 4 cm^{-1} in resolution. Liquids were analysed with a Thermo Scientific DXR Raman Microscope apparatus. The spectra were collected by recording 32 scans in the range 1300–300 cm^{-1} with a resolution of 5 cm^{-1} using a laser of 532 nm with a power of 10 mW.

Diffuse reflectance ultraviolet-visible spectroscopy (DR-UV-Vis) was recorded in a Shimadzu UV-3600 plus apparatus equipped with a Harrick Praying Mantis diffuse reflection accessory. The background of the samples was referenced to a BaSO₄ pellet material and recorded from 600 to 190 nm wavelength range with a sample interval of 0.5 nm and a slit width of 2 nm. The reflectance values were automatically transformed to Kubelka-Munk with the integrated software UVProbe 2.62.

³¹P NMR analyses were recorded at room temperature (295 K) on a Bruker Avance 500 operating at 11.7 T (202 MHz for ³¹P). Experiments were run under TopSpin program (Bruker) using a BBO{¹H,X} probehead equipped with a z-gradient coil. Quantitative ³¹P NMR analyses were carried out by using the standard Bruker zg pulse program with an acquisition time of 1.6 s, collecting 16 scans and applying a relaxation delay of 45 s.

Catalytic experiments

The catalytic tests were carried out at 70 °C under air in a closed 10 mL round-bottomed two-neck flask reactor equipped with a reflux condenser, oil bath, and magnetic stirring rod (500 rpm). Typically, the reactor was loaded with the catalyst (mass adjusted to 0.02 mmol of W atoms in the reactor); solvent CH₃CN (9.59 mL); internal standard dibutyl ether (1 mmol); 30 wt% aq H₂O₂ (1 mmol); and cyclooctene (1 mmol). Before olefin addition, the reaction was pre-heated at the desired reaction temperature; the reaction time was counted immediately after olefin addition. The catalytic reaction was monitored every hour using a Shimadzu GC-2010 PLUS equipped with a capillary column (Shimadzu SH-Rtx-1 15 m x 0.25 mm), and a flame ionization detector. Assignments of reagents and products were made by comparison with authentic samples. All tests were treated with estimated standard deviation, which was less than 3% in all cases. Hot filtration tests, to investigate the possibility of leaching of active species from the solids to the reaction liquid medium, were carried out under typical catalytic conditions for 2 h after which the solid was separated from the reaction medium by filtration with a syringe equipped with a 0.2 μm VWR membrane filter. The evolution of the remaining solution was subsequently monitored by GC, at 70 °C. Post-characterization tests after the first catalytic cycle were carried out by evaporating the reaction mixture to dryness at 70 °C. Subsequently, the remaining residual solid was employed as such for further characterization analysis.

Results and discussion

As we previously reported [34], reaction of Keggin H₃PW₁₂O₄₀ (PTA) with bipyridine is beneficial for the catalytic epoxidation of cyclooctene if PTA is pre-activated with H₂O₂ before reacting with 2, 2'-bpy or 4,4'-bpy. The pre-activation yielded two "pre-activated compounds" composed of peroxotungstate moieties without a Keggin structure. The pre-activated compounds were considerably more active than their Keggin-based analogues (i.e., (2,2'-Hbpy)₃[PW₁₂O₄₀] and (4,4'-H₂bpy)_{1.5}[PW₁₂O₄₀]·1.5H₂O) in which PTA directly reacts with bipyridine. In the present study, the structure, identity, and catalytic properties of the pre-activated compounds are further investigated. In addition, two additional pre-activated compounds are prepared. In this case, the pre-activation of PTA with H₂O₂ is followed by the addition of a phosphorus source (H₃PO₄) with the aim of increasing the concentration of PW₄ species [20]. The synthesis of the four compounds (Scheme 1) was carried out by stoichiometrically reacting an aqueous mixture of H₃PW₁₂O₄₀/H₂O₂/H₃PO₄ (ratios 1:100:2, method (a)) with solid 2, 2'-bpy (**a-22**) or 4,4'-bpy (**a-44**) (ratios 3:1.5), or reaction of

H₃PW₁₂O₄₀/H₂O₂ (ratios 1:100, method (b)) with solid 2,2'-bpy (**b-22**) or 4,4'-bpy (**b-44**) (ratios 3:1.5). Quantities were based on the measured pH (pH = 0.63) of the PTA solution and pK_a values of monoprotonated 2, 2'-bpyH⁺ / 4,4'-bpyH⁺ (pK_{a2} = 4.4/4.9 [35]) and diprotonated 2, 2'-bpyH₂²⁺ / 4,4'-bpyH₂²⁺ (pK_{a1} = -0.2/2.5 [35]) species.

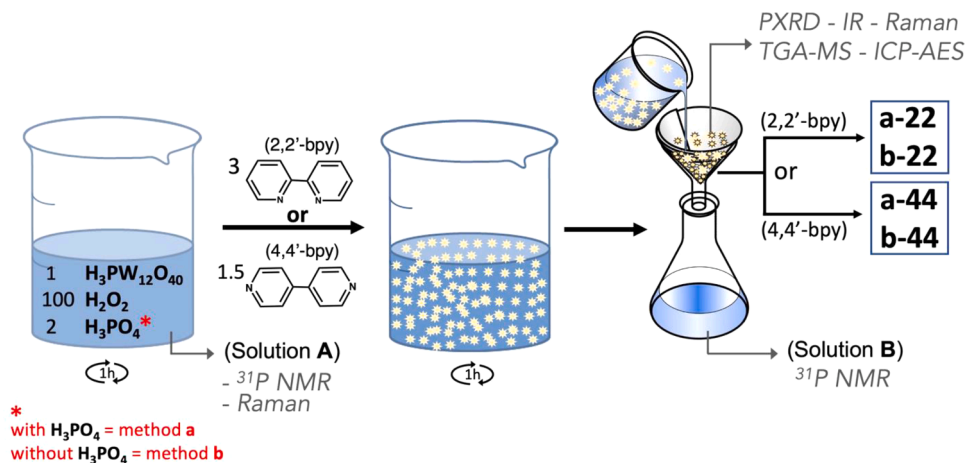
Analysis of the solid compounds

PXRD analysis was performed to verify the formation of the compounds. In all cases, they showed new emerging diffraction lines when compared to their respective precursors (Fig. S1), confirming the effective structural integration of both organic and inorganic units in a new crystal lattice. The diffraction lines of **a-22** and **b-22** (Fig. 1) indicate that they are structurally very similar, regardless of their different preparation methods (with and without H₃PO₄ addition). On the contrary, the structures of **a-44** and **b-44** appear different, indicating that the synthetic methodology produces a change in the structural framework of the compounds when the 4,4'-bpy isomer is used.

The catalytic properties of the compounds were tested in the epoxidation of cyclooctene with H₂O₂ and compared with IV-PW₄ prepared according to Venturello et al. [7] (see experimental). The compounds built from the isomer 2,2'-bpy show superior activities than those containing 4,4'-bpy (Fig. 2). The structural similarity of **a-22** and **b-22** is not mirrored in their catalytic behaviour as **a-22** is substantially more active than **b-22**. Conversely, the structurally different **a-44** and **b-44** exhibit lower but similar catalytic activities. On the other hand, IV-PW₄ displays high activity only during the first hour but then rapidly deactivates and exhibits the poorest activity at the end.

The thermal stability of the compounds was examined by TGA-MS (Fig. 3). The isostructural **a-22** and **b-22** present different thermal profiles. The most significant weight loss takes place in stage 1 where **a-22** (23.3%) loses less weight than **b-22** (25.7%) up to 200 °C. Between 200 and 550 °C (stage 2) **a-22** (15.0%) and **b-22** (15.2%) display similar weight losses that are identified, in both stages, as due to evolutions of H₂O and CO₂. Above 550 °C, the residual inorganic content of **a-22** (62.2%) is higher than that of **b-22** (59.2%) in agreement with the elemental analysis displayed in Table S1. Besides, Table S1 also shows that **a-22** presents an atomic weight content of W and P superior than that of **b-22**, as expected. Considering that both compounds have the same crystalline structure, the additional content of W and P could be related to an amorphous phase present in low quantities in **a-22**, and not (or less) in **b-22** (see inset of Fig. 1).

The thermogravimetric profiles of **a-44** and **b-44**, on the other hand, appear different from those of **a-22** and **b-22**. In stage 1, the weight losses up to 200 °C of **a-44** (15.2%) and **b-44** (11.9%) are lower than **a-**



Scheme 1. Illustration of the synthesis and characterization steps of compounds **a-22** (H₃PW₁₂O₄₀/H₂O₂/H₃PO₄ + 2,2'-bpy), **b-22** (H₃PW₁₂O₄₀/H₂O₂ + 2,2'-bpy), **a-44** (H₃PW₁₂O₄₀/H₂O₂/H₃PO₄ + 4,4'-bpy), and **b-44** (H₃PW₁₂O₄₀/H₂O₂ + 4,4'-bpy).

22 (23.3%) and **b-22** (25.7%) and only an evolution of H₂O is detected. From 200 to 600 °C, **a-44** (23.8%) releases a mixture of H₂O and CO₂ in a succession of overlapping events, whereas **b-44** (23.2%) only emits CO₂.

Above 600 °C, the inorganic content of **b-44** (64.8%) is higher than **a-44** (60.9%), which is also in agreement with the elemental analysis (Table S1). In summary, the elemental and thermogravimetric results show that all compounds present different compositions, with in particular, their W and P atomic concentrations not being equivalent. The thermal fragmentations of compounds built from 2,2'-bpy and 4,4'-bpy are substantially different, which echoes their structural and catalytic differences.

A direct correlation between epoxidation activity and phosphorus content is observed. The compounds with a high phosphorus content appear more active in the epoxidation reaction. Notice that the quantity of all the catalysts engaged in the tests was normalized to the number of W atoms (i.e., 0.02 mmol of W) making that the phosphorus content in the respective tests is not the same. For instance, **a-22** (prepared with addition of H₃PO₄) considered isostructural with **b-22** (prepared without addition of H₃PO₄) presents a higher concentration of phosphorus and, with the same W loading in the reactor, is significantly more active. Method (a), however, shows to increase only the phosphorus content of compounds formed with 2,2'-bpy whereas it leads to lower phosphorus content with 4,4'-bpy. Note that, during the first 8 h, the activity of **a-44** (wt.% P = 0.02) is slightly higher than that of **b-44** (wt.% P = 0.07). However, the latter is more active after 24 h, which supports the observed correlation. Nevertheless, the phosphorus/activity relationship seems to apply only to compounds based on bipyridine and not to IV-PW₄ Venturello's hybrid, which, let us remind it, despite having the highest phosphorus content (Table S1) shows the poorest catalytic activity (Fig. 2).

To collect information about the functional groups present in the compounds, the samples were examined by IR and Raman spectroscopies. The vibrational assignments of the anionic skeleton structures of the compounds were ascribed based on the known vibrational data of the PW₄ anion of IV-PW₄ and related anionic peroxotungstate species (Table 1).

The IR and Raman spectra of the four compounds and IV-PW₄ present several bands due to their associated organic ligands whose spectral comparison is shown in Figs. S3–S6. In the low-frequency region of Fig. 4 (ca. 1150–400 cm⁻¹), the IR bands of the anionic skeleton of IV-PW₄ show the presence of P-O (1088, 1049 cm⁻¹), W=O (971 cm⁻¹), O-O (841 cm⁻¹), and W(O₂) groups (area marked in yellow). Based on the crystal structure of IV-PW₄, these bands correspond to four WO(O₂)₂ units linked by a central tetrahedral PO₄ moiety [7]. On the other hand, the spectra of **a-22** and **b-22** appear almost identical but vary from that of IV-PW₄. In the P-O region (ca. 1150–1100 cm⁻¹), both compounds

display only weak bands of 2,2'-bpy ligand at 1037 cm⁻¹. Below 1100 cm⁻¹ (areas highlighted in grey on Fig. 4), three bands are tentatively assigned as W=O, O-O, and W(O₂) groups whose vibrational positions shift to lower wavenumbers relative to IV-PW₄ (see bands listed in Table 1). The spectra of **a-44** and **b-44**, which also contain W=O, O-O, and W(O₂) groups, present less resemblance between them than the resemblance between **a-22** and **b-22** spectra. **b-44** for instance, exhibits a strong broad band centred at 790 cm⁻¹ that masks the vibrational region of the O-O group, but it clearly shows bands associated to W=O and W(O₂) groups respectively at 953 and 517 cm⁻¹. On the other hand, **a-44** displays a distinguishable O-O band at 826 cm⁻¹ accompanied with bands of W=O, and W(O₂) groups respectively at 953 and 525 cm⁻¹, which apart from W=O, vibrate at higher frequencies relative to **b-44**. The Raman spectrum of IV-PW₄ (Fig. 5) displays the typical bands associated to its WO(O₂)₂ moieties (Table 1); however, the bands attributed to the tetrahedral central PO₄ group expected at ca. 1036–1065 cm⁻¹ are not visible [10].

In the low-frequency region, the Raman bands of **a-22** and **b-22** at 947, 848, 594 and 550 cm⁻¹ are almost identical and clearly show the presence of W=O, O-O, and W(O₂) groups respectively which, similar to IR, vibrate at lower frequencies with respect to IV-PW₄. Typically, bands located between 500 and 600 cm⁻¹, as reported for oxidiperoxo complexes of molybdenum and substituted bipyridine [43] or pyrazolopyridine [44] ligands, correspond to the stretching modes of M(O₂)₂ (M=Mo, W) groups. Therefore, we suggest that the anions of **a-22** and **b-22** are composed of oxidiperoxo tungstate WO(O₂)₂ moieties. The Raman spectrum of **b-44** displays a sharp line associated with the vibration of an O-O group at 846 cm⁻¹, including the band W=O at 952 cm⁻¹ and W(O₂) at 556 cm⁻¹, and thus confirms that the anion is composed of WO(O₂)₂ moieties. The same vibrational groups appear for **a-44** but are slightly shifted to higher wavenumbers compared to **b-44**. Based on the vibrational data of the compounds in the low-frequency region, the presence of a Keggin PW₁₂ structure is excluded as no bands of P-O, W=O_t, W-O_c-W, and W-O_e-W in IR [45,46], nor W=O_t in Raman are observed [45]. This is consistent with the PXRD analysis (Fig. S1) of the compounds with their respective Keggin PW₁₂-based analogues (2,2'-Hbpy)₃[PW₁₂O₄₀] and (4,4'-H₂bpy)_{1.5}[PW₁₂O₄₀]·1.5H₂O [34] where no diffraction agreement is observed. The protonation state of the hybridized bipyridine ligands was examined in the IR and Raman mid-frequency regions (ca. 1700–1500 cm⁻¹). Generally, bands above 1600 cm⁻¹ are typical of protonated pyridyl rings, and bands between 1550 and 1600 cm⁻¹ are characteristics of neutral rings [35].

The IR of hybridized 4,4'-bpy samples show the pyridyl rings vibrating at 1628 cm⁻¹ with a shoulder at 1588 cm⁻¹ (pink and light blue sections in Fig. 4). The compounds were compared with neutral and protonated bipyridine species (Figs. S3 and S4) confirming that the hybridized 4,4'-bpy ligands in **a-44** and **b-44** are protonated. On the other hand, the pyridyl rings of hybridized 2,2'-bpy in **a-22** and **b-22** appear vibrating at the boundary between protonated and neutral species. Raman, which can provide information about the conformation and protonation of bipyridine, shows the vibration of pyridyl rings in hybridized 2,2'-bpy and 4,4'-bpy at 1602 and 1644 cm⁻¹ respectively (Fig. 5). Based on the spectral Raman comparison between protonated and neutral bipyridine species (Figs. S5 and S6) the ligands in **a-44** and **b-44** were identified as 4,4'-bpyH₂⁺ species. On the other hand, the Raman spectra of **a-22** and **b-22** suggest that the hybridized 2,2'-bpy ligands, which exhibit an intermediate character between protonated and neutral species, are likely to be in a coordinated mode, as observed in earlier vibrational studies of 2,2'-bpy adsorbed on silica, alumina, zirconia and titania [47,48]. Complementary C and N elemental analyses of the compounds show that the W/N molar ratios of **a-44** and **b-44**, vs **a-22** and **b-22** are different (Table S1). For example, the ones composed of 2,2'-bpy (W/N of **a-22** = 0.6 and W/N of **b-22** = 0.5) contain one bipyridine per tungsten atom, i.e., one 2,2'-bpy per WO(O₂)₂ moiety, whereas those made of 4,4'-bpy present 1/2 bipyridine per WO(O₂)₂ moiety. Therefore, it is likely that the W center of the

Table 1
Vibrational spectroscopic data in the low-frequency region (cm⁻¹).^a

Compound	$\nu(\text{W}=\text{O})$	$\nu(\text{O}-\text{O})$	$\nu_{\text{as}}, \nu_{\text{s}}(\text{W}(\text{O}_2))$	$\nu(\text{P}-\text{O})$	Refs.
IV-PW ₄	971	841	571	1088	[8]
			526	1049	
	984	858	592		[10]
			575		
a-22	940	833	540		[9,10,36–39]
	947	848	594		
			550		
			550		
b-22	940	833	540		
	947	848	594		
			550		
			550		
a-44	953	826	525		
	957	848	561		
			517		
b-44	953		517		
	952	846	556		

^a Raman data in italics; bands due to ligands are not listed.

oxodiperoxo moiety in **a-22** and **b-22** directly coordinates with a N, N'-chelated 2,2'-bpy. Isomer 4,4'-bpy, on the other hand, does not directly coordinates with the metal center, presumably due to its structure which does not allow a *cis* or *trans* conformation, making that it cannot act as a tweezer organic ligand.

In summary, the vibrational examination indicates that compounds **a-22** and **b-22** present the same anion structures containing $\text{WO}(\text{O}_2)_2$ moieties likely coordinated with 2,2'-bpy. On the other hand, the nature of **a-44** and **b-44**, also composed of $\text{WO}(\text{O}_2)_2$ moieties, appears to be ionic as the ligands are protonated (4,4'-bpy H_2^+ species) and therefore, interact electrostatically with the anion. Unlike IV-PW₄, our four compounds only display weak bands of bipyridine in the P-O region, which may indicate that the hybridized anionic structures are less condensed (smaller or less confined atomic assembly) than Keggin PW₁₂ or PW₄ anions. As matter of fact, the presence of a PO_4^{3-} tetrahedral unit typically allows a greater assembly of more than one $\text{WO}(\text{O}_2)_2$ moiety. These results, therefore, suggest that the observed relationship between activity and phosphorus content may not be the only factor to consider, as the nature of the compounds may also play a role in the catalytic reaction. The difference in the number of bipyridines per $\text{WO}(\text{O}_2)_2$ unit obtained by selecting 2,2'-bpy or 4,4'-bpy, which in principle makes the **a-22** and **b-22** group more hydrophobic than **a-44** and **b-44**, could also influence how the compounds interact with the hydrophobic olefin and the less hydrophobic epoxide product.

The electronic properties of the compounds and IV-PW₄ were analysed by DR-UV-Vis in order to collect the reduction potential (oxidation power) and relate it with the catalytic activity. The samples were initially measured in diffuse reflectance (DR) and later transposed to Kubelka-Munk function $F(R_\infty)$ to obtain absorption values which are attributed to the ligand-metal charge transfer (LMCT) $\text{O}^{2-} \rightarrow \text{W}^{6+}$ [49–51] (Fig. S7). This allowed the Tauc's relation $[F(R_\infty)h\nu]^{1/2}$ vs. photon energy to be applied and obtain the band gap energy (E_g) which is associated with the reduction potential [52–54]. The E_g values were determined by finding the energy intercept of a straight-line drawn tangent to the inflection point of the curves (Fig. 6). IV-PW₄ has the highest E_g value, i.e., presents the lowest reduction potential (lowest oxidative power) which, compared to the compounds, increases in the order IV-PW₄ < **a-22** < **b-22** < **b-44** < **a-44**. In other words, the most catalytically active **a-22** displays the lowest oxidative power and the less active **a-44** the highest. It is generally accepted that the catalytic oxidation of organic substrates by hydrogen peroxide involving transition metals proceeds primarily via a heterolytic mechanism. In other words, it does not necessarily involve a change in the oxidation state of the metal, rather, the substrate is oxygenated in the coordination sphere of the metal complex, and decomposes to give the epoxide and the metal dioxo complex [55–57]. Interestingly, aside from IV-PW₄, the E_g values of the compounds, as well as their phosphorus content (Table S1) and catalytic activity (Fig. 2, at 24 h) rise in the same sequence (**a-44** < **b-44** < **b-22** < **a-22**).

In short, the characterization of the compounds demonstrates that the most active catalysts are those with the highest phosphorus content, highest E_g (i.e., lowest reduction potential and thus lowest oxidation power), and non-ionic character (coordinated). This correlation does not apply to IV-PW₄ of Venturello, as it is the species with the highest E_g and phosphorus content but exhibiting the weakest catalytic activity.

To investigate the poor performance of IV-PW₄ under the employed catalytic conditions, the solid, collected via evaporation of the homogeneous catalytic mixture after the first run (see experimental), was analyzed by IR (Fig. S8). The spectrum displays strong sharp bands of the counter-cation (tetrahexylammonium) at 1454 and 1372 cm^{-1} and a set of weak unidentified bands in the low-frequency region (1126–400 cm^{-1}) where the PW₄ anion vibrates. When compared to the anionic bands of fresh IV-PW₄ (in the low-frequency region) it can be deduced that the PW₄ structure of the spent IV-PW₄ catalyst was altered. The absence of the anionic vibrational bands of the spent catalyst suggests that the anion was not efficiently reoxygenated by H_2O_2 under the

employed catalytic conditions. Furthermore, judging from its catalytic profile (Fig. 2), the high activity displayed during the first hour (similar to the most active **a-22**) is likely due to the complete exhaustion of its structurally active peroxo oxygens that later, unlike **a-22**, were not efficiently regenerated by H_2O_2 . Notice that in our system, the $\text{H}_2\text{O}_2/\text{W}$ molar ratio (50/1) is higher than those of Ishii et al. [5] (~31/1), and Venturello et al. [7] (~40/1), therefore, there is in principle sufficient H_2O_2 to stoichiometrically regenerate the PW₄ anion of IV-PW₄ after the oxygen transfer forming the epoxide, and make the process catalytic. However, contrary to the biphasic catalytic conditions employed by Ishii-Venturello, in our monophasic system, the anion PW₄ of IV-PW₄ coexists in the same phase as aqueous H_2O_2 , where the rate of the catalyst regeneration may have been affected or hampered by (i) the high hydrophobicity of the associated cation ($(\text{C}_6\text{H}_{13})_4\text{N}^+$), (ii) solvation of the hydrophilic PW₄ anion by water ($\text{H}_2\text{O}_2/\text{H}_2\text{O} = 30/70\%$) or by the dipolar aprotic solvent CH_3CN . This is not the case for the bipyridine-based compounds. As determined by IR, the anionic structures of the compounds are retained after the first catalytic cycle (Fig. S9), proving that the reaction proceeds catalytically. Furthermore, hot filtration tests (see experimental section) carried out for **a-22**, **b-22**, **a-44**, and **b-44** revealed that the catalysis occurs mainly in the homogeneous phase as much of the activity was detected after removing the apparent insoluble powders by filtration. Additional experiments to investigate the effect of H_2O_2 in the catalytic medium were conducted. The most catalytically active **a-22** and **a-44** were tested in the epoxidation in absence of H_2O_2 . When H_2O_2 was not present, the activities of **a-22** and **a-44** dropped dramatically in contrast to when H_2O_2 was present in the reaction medium (Fig. S10). To post-characterize in the solid state the samples tested in absence of H_2O_2 after the first catalytic cycle, the catalytic mixtures were first hot-filtrated (by removing the solids after 2 h) and then evaporated to dryness. The remaining residual paste (ca. 1.5 mg) was then analyzed by Raman (Fig. S11). The spectra clearly show the lack of O-O and $\text{W}(\text{O})_2$ bands in both cases compared to their respective fresh equivalents. On the other hand, the terminal oxo ($\text{W}=\text{O}$) and bipyridine ring stretching bands are shown shifted to lower wavenumbers, presumably due to the altered structures of the anions. To check whether the structure of the compounds was irreversibly degraded by running the reaction without H_2O_2 after the first catalytic cycle, the residual paste was exposed to fresh H_2O_2 and then analyzed by PXRD. This was accomplished by mixing for 1 h at 70 °C an excess of H_2O_2 (~5 mL of H_2O_2 per 1–2 mg of solid) with the leftover paste and subsequently evaporating the mixture to dryness under vacuum at room temperature. The diffractograms of the two samples display an overall amorphous phase in contrast to the well-defined diffraction peaks of their fresh counterparts (Fig. S12). Therefore, the presence of H_2O_2 in the catalytic medium appears pivotal not only in terms of epoxidation activity but also in the structural preservation of the catalytic material itself. These findings also open new questions from a catalytic point of view. In this case H_2O_2 does not seem to act as a simple reoxygenating agent as proposed by Mimoun et al. [55,56] and Sharpless et al. [58] in the 1970s or by more recent theoretical studies [59]. The fact that the compounds are catalytically incompetent in the absence of H_2O_2 and then unable to regenerate or “repair” their structural peroxo groups with fresh H_2O_2 , argues in favor of the existence of a different mechanism. Based on this reasoning, we hypothesize that H_2O_2 itself could be the species that likely catalyzes (directly or indirectly) the epoxidation reaction, as the mechanism proposed by Thiel et al. [60,61] and later studies [62] where H_2O_2 forms an active intermediate species with the peroxo catalyst (i.e., a hydroperoxo intermediate species), that is believed to be the true active species.

Additionally, we noticed that, under typical catalytic conditions (and with H_2O_2), the hot-filtrated mixture of **a-22** showed the presence of white solid particles inside the reactor after 24 h of reaction. The solid was separated by centrifugation and analyzed by PXRD (Fig. S13). The analysis revealed that the structure of the collected precipitate is equivalent to the corresponding fresh **a-22**. This demonstrates that the

dissolution of the catalyst in the reaction medium is temporary, and eventually that the catalyst returns to an insoluble state without structural changes. Limited by the traces of precipitated material obtained, which makes its collection, washing and weighing difficult, it was not possible to recycle the catalyst in a second catalytic cycle.

Nevertheless, to further explore the cause of this last precipitation, in a control experiment, the catalytic mixtures of **a-22** and **b-22** (without addition of olefin) were hot-filtered after 2 h of reaction and immediately transferred to a new vessel in which they were allowed to stand at ambient temperature for 1 week. As no sign of precipitation was observed, the same experiment was repeated, but this time 1 mmol of the epoxide (equivalent to 100%C) was added to each vessel immediately after hot filtration. After standing for 24 h at room temperature, the vessel containing **a-22** showed the presence of white particles that were later identified by PXRD as fresh **a-22**. At the opposite, 7 days were required for the soluble particles of **b-22** to precipitate. These control experiments prove that the precipitation of the catalysts is caused by the produced epoxide. Finally, with the information gained through the analysis of the solid, the study was extended to analyse the aqueous solutions before (solution A) and after (solution B) ligand addition by means of liquid Raman and ^{31}P NMR spectroscopies.

Spectroscopic analysis of solution A

In order to monitor the degradation of the PW_{12} precursor with H_2O_2 , and thus identify the peroxo species that are formed, the aqueous solution A was analysed *in situ* by Raman spectroscopy (Fig. 7). The aqueous solution was monitored over a period of 125 min and measured at intervals of 10 min. For every interval of 10 min five scans were recorded (i.e., one scan every 2 min; see groups of black and grey lines in Fig. 7). The starting PW_{12} solution (highlighted in blue) shows two bands at 1012 and 995 cm^{-1} due to the $\nu_s(\text{W}=\text{O})$ and $\nu_{as}(\text{W}=\text{O})$ terminal oxygen vibrations [63] (see drawing of PW_{12} structure), whereas H_2O_2 (black line in bold) displays a single strong signal at 876 cm^{-1} . After 1 min of reaction, the bands associated with the PW_{12} structure and H_2O_2 start rapidly to decrease during the measurement (5 scans). At the same time, six bands emerge at 965, 854, 647, 619, 559, and 321 cm^{-1} attributed to $\nu(\text{W}=\text{O})$, $\nu(\text{O}-\text{O})$, $\nu(\text{PO}_4)$, $\nu_{as}(\text{W}(\text{O}_2))$, $\nu_s(\text{W}(\text{O}_2))$, and $\nu(\text{W}(\text{OH})_2)$ groups respectively [9]. After 30 min, the PW_{12} bands disappear completely indicating that the PW_{12} structure was completely degraded. Between 30 and 60 min, all bands remain stable without appreciable changes. Addition of H_3PO_4 after 60 min (and measured at 70 min) causes a shift on the $\nu(\text{W}=\text{O})$ band from 965 to 969 cm^{-1} (see inset (a)). Besides, the intensity of the $\nu_{as}(\text{W}(\text{O}_2))$ signal at 619 cm^{-1} (see inset (b)) decreases, while the intensity of the scarcely visible band of $\nu(\text{PO}_4)$ at 647 cm^{-1} increases.

The recorded *in situ* spectra indicate that under our synthesis conditions, the polyanionic structure of the PW_{12} precursor is completely degraded by H_2O_2 after 30 min. The rapid initial decrease of the H_2O_2 signal and simultaneous formation of new peroxo species, evidence the high dynamic rate at which the PW_{12} structure is degraded. The systematic vibrational shift of the emerged $\text{W}=\text{O}$ signal and decrease of the $\text{W}(\text{O}_2)$ band after addition of H_3PO_4 , suggest that the concentration of the peroxo species changed (a more detailed examination on these shifts is provided below by ^{31}P NMR in Fig. 8). In addition, the increased signal of $\nu(\text{PO}_4)$ at 647 cm^{-1} which remains after the addition of H_3PO_4 , implies that there is a portion of H_3PO_4 that did not react. The fact that the new peroxo species emerged at lower wavenumbers relative to PW_{12} confirms the formation of peroxide clusters that contain a smaller number of tungsten atoms [9]. The bands of these new aqueous peroxo species, which are present prior reaction with bipyridine, also coincide with the Raman bands of the compounds in the solid state (Fig. 5). Finally, the fact that Raman spectroscopy is not capable of distinguishing between different peroxometalate species in a mixture, but instead, provides the total sum of vibrations of a family of peroxo species, prompted us to investigate the complex speciation of solution A by ^{31}P

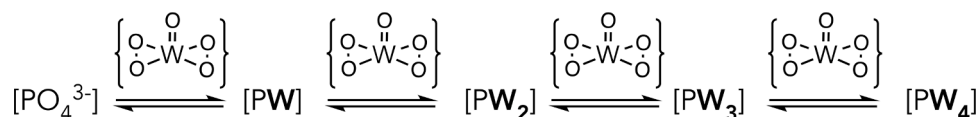
NMR.

$\text{H}_3\text{PW}_{12}\text{O}_{40}$ and H_3PO_4 (in absence of H_2O_2 to prevent the degradation of the PW_{12} structure) were initially analysed in order to distinguish their individual resonance signals under our synthesis conditions. The resonance signal of $\text{H}_3\text{PW}_{12}\text{O}_{40}$ appears as a singlet at -14.8 ppm in the most shielded part of the spectrum while at the opposite side, H_3PO_4 shows a singlet at 0.37 ppm (Fig. 8a).

The H_3PO_4 signal is upfield-shifted from 0.37 to -0.24 ppm when combined with H_2O_2 in the absence of PW_{12} (Fig. 8b). The aqueous system $\text{H}_3\text{PW}_{12}\text{O}_{40}/\text{H}_2\text{O}_2$, immediately analysed after 1 h of reaction (Fig. 8c), displays four lines that, based on their chemical shifts, $^2J_{\text{W-P}}$ coupling constants, and relative intensities of the satellites with respect to the central line (see details in Table S2), were identified as PW , PW_2 , PW_3 , and PW_4 species in close agreement with earlier studies [10,11]. Interestingly, to obtain well-resolved satellites and permit an unambiguous assignment of the different PW_n ($n = 1-4$), the spectra acquisition was fixed to 16 scans since at lower numbers the $^2J_{\text{W-P}}$ satellites did not have sufficient resolution, and at higher numbers, the satellite lines were severely broadened and flanked by unresolved humps. The satellite resolution problem was primarily due to the formation of paramagnetic oxygen bubbles in the NMR tube, which affected the resolution of the spectra. The displayed four PW_n species, and the absence of signals due to the resonances of PW_{12} and PO_4^{3-} species, corroborate the Raman kinetic data (Fig. 7) demonstrating that the structure of the PW_{12} precursor is fully degraded after 1 h of reaction, and that at the same time, new PW_n peroxo species are formed. Let us recall that the degradation of PW_{12} also generates inorganic peroxotungstates by-products without phosphorus, which are typically detectable by ^{183}W NMR [9,11] and thus, are also present in the $\text{H}_3\text{PW}_{12}\text{O}_{40}/\text{H}_2\text{O}_2$ system. Upon addition of H_3PO_4 to the $\text{H}_3\text{PW}_{12}\text{O}_{40}/\text{H}_2\text{O}_2$ system (Fig. 8c), the relative intensities of the mono-, bi-, tri- and tetranuclear PW_n species increase.

The use of trimethyl phosphate (TMP) as internal standard (decuplet at $\sim 3.5-2.6$ ppm) allowed to integrate the relative intensities of the phosphorus signals to compare the spectra before and after the addition of H_3PO_4 . The integrated signals show that the concentration of PW_n species increases in the order $\text{PW}_4 < \text{PW}_3 < \text{PW}_2 < \text{PW}$ when H_3PO_4 is added (inset of Fig. 8). In other words, the increment is higher for species with richer phosphorus content (less W atoms). For example, the concentration of PW increases more than 3 times over PW_4 and 2 times over PW_3 . Furthermore, the appearance of a small singlet at -0.32 ppm due to the resonance of PO_4^{3-} is consistent with the Raman signal of $\nu(\text{PO}_4)$ at 647 cm^{-1} , which also increases upon addition of H_3PO_4 (Fig. 7, inset (b)). This indicates that either, a fraction of the 2 mmol of H_3PO_4 added to the $\text{H}_3\text{PW}_{12}\text{O}_{40}/\text{H}_2\text{O}_2$ system does not react and remains in excess, or that some remaining H_3PO_4 is fully consumed and stays in equilibrium with the four PW_n species (see Scheme 2). Additionally, the fact that H_3PO_4 causes a change in the PW_n concentration also agrees with the systematic Raman shift of the $\nu(\text{W}=\text{O})$ bands (Fig. 7, inset (a)) when H_3PO_4 is added after 1 h of reaction, which appears to be caused by the unequal increased of peroxo species holding a tungsten-oxygen double bond. In short, the ^{31}P NMR spectra of Fig. 8 reveals that there are four different phosphorus species present before bipyridine is added to solution A (method (b)). Addition of H_3PO_4 (method (a)) does not generate additional phosphorus species. Rather, it increases the concentration of the pre-existing PW_n species, preferentially those with fewer W atoms. Moreover, the amount of H_3PO_4 added shows to be partially consumed, a part likely remaining in equilibrium with the PW_n species. Finally, the synthesis methodologies (a) and (b) differ primarily in terms of concentration of PW_n species.

Examination of the filtrate solution B (Scheme 1) by ^{31}P NMR was conducted in order to analyse the residual phosphorus species that were not hybridized, and thereby indirectly identify the precipitated PW_n species that were collected by filtration. This is based on the assumption that if a certain phosphorus species is selectively precipitated (consumed) by a matching ligand, the intensity of its resonance signal, in



Scheme 2. Representation of the PW_n species likely coexisting in fast equilibrium and possibly interconverted through $\{\text{WO}(\text{O}_2)_2\}$ units (inspired from [65,66]).

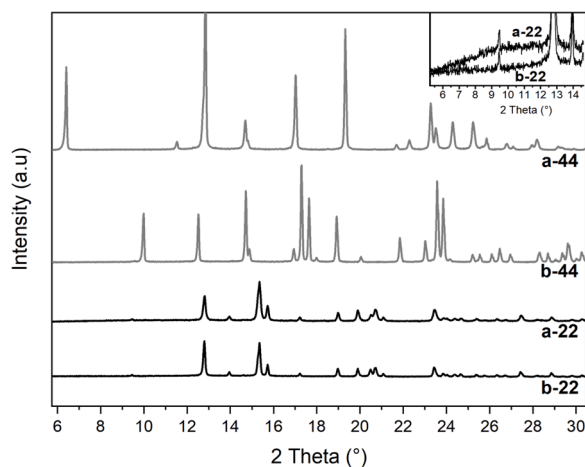


Fig. 1. PXRD patterns of compounds a-22, a-44, b-22, b-44. The inset plot compares b-22 and a-22 at low theta angle.

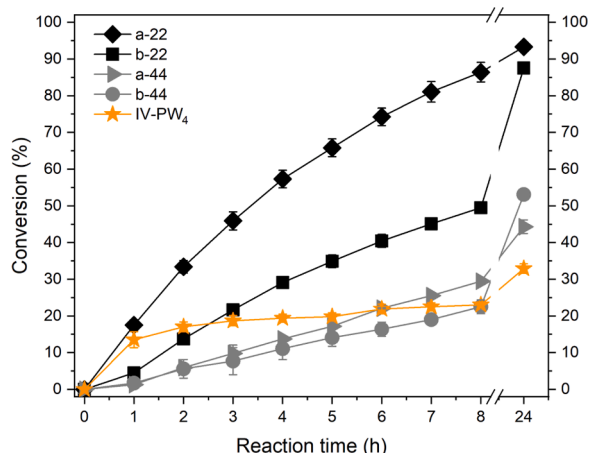


Fig. 2. Epoxidation of cyclooctene catalyzed by a-22, b-22, a-44, b-44, and IV- PW_4 compounds. Reaction conditions: molar ratios $\text{W}:\text{olefin}:\text{H}_2\text{O}_2 = 1:50:50$, in CH_3CN at 70°C . All tests showed $> 99\%$ selectivity towards cyclooctene oxide. Separation of the reaction mixture by GC is shown in supplementary (Fig. S2).

the aqueous solution, should decrease proportionally to the amount precipitated. The two-component association system ($\text{H}_2\text{WO}_4/\text{H}_3\text{PO}_4$) of Venturello [7] was first analysed to afterwards use it as reference system to then investigate our compounds with bipyridine, as the quaternary ammonium salt tetrahexylammonium chloride (THACL) was shown to selectively isolate the PW_4 anion of Venturello [8]. The aqueous system $\text{H}_2\text{WO}_4/\text{H}_2\text{O}_2/\text{H}_3\text{PO}_4$ of Venturello (Fig. 9a) displays four phosphorus resonances of which one is as a singlet and three are triplets with well-resolved satellites. Analysis of intensities and coupling constants of the tungsten satellites showed different values compared to the $\text{H}_3\text{PW}_{12}\text{O}_{40}/\text{H}_2\text{O}_2/\text{H}_3\text{PO}_4$ system, however, the data showed to follow the same trend.

The species with more tungsten atoms (e.g., $\text{PW}_4 > \text{PW}_2$) present the most shielded values (towards more negative displacement), longest $^2J_{\text{W-P}}$ coupling constants, and highest percentage of satellites/central

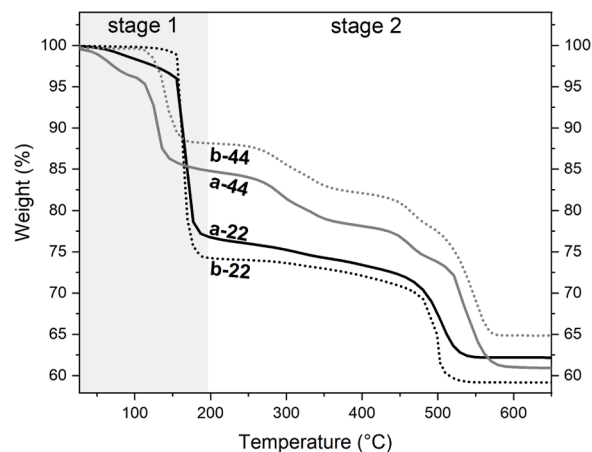


Fig. 3. TGA profiles of the four compounds (under air, $10^\circ\text{C}/\text{min}$).

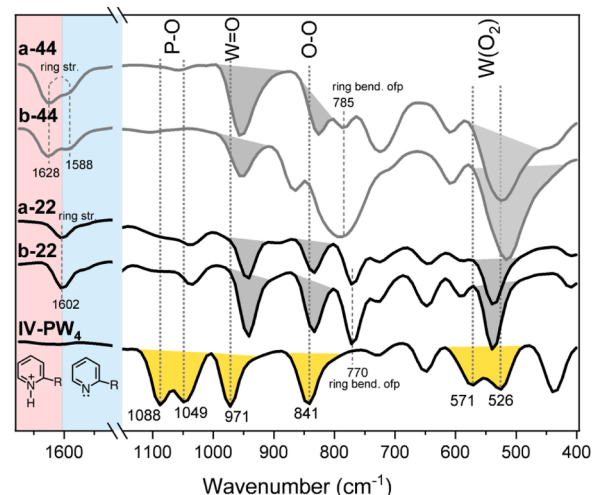


Fig. 4. IR spectra of the four compounds and IV- PW_4 in the mid- and low-frequency regions. Abbreviations: bend. stands for bending, ofp stands for out-of-plane (band assignment of ligand from [40,41]).

line ratios (see details in Table S2). Therefore, the resonance signals were identified, from high to low frequency as PO_4^{3-} , PW_2 , PW_3 and PW_4 species. Notice that in this system the PW species is absent. The filtrate solution, obtained after filtrating the precipitated PW_4 (i.e., IV- PW_4), shows the same four signals as the fresh solution but with different intensities (Fig. 9b). Comparison of the integrated signals of each spectrum (inset Fig. 9) reveals that in the filtrate solution, the concentration of the PW_n species was decreased in the order $\text{PW}_4 > \text{PW}_3 > \text{PW}_2$, while the concentration of the uncoordinated PO_4^{3-} ion was increased. As expected, the ^{31}P spectrum of the collected precipitate IV- PW_4 (solubilized in $\text{CD}_3\text{CN}/\text{CDCl}_3$ (9:1)) appears as pure PW_4 (see inset of Fig. S14, and W/P in Table S1) with no traces of PW_3 or PW_2 species presumably present in the solid (based on its diminished integrals).

In order to rule out the possibility that PW_3 and PW_2 species actually precipitated but were washed off or removed as impurities in the IV- PW_4 recrystallization process, the solid was analysed as such, without

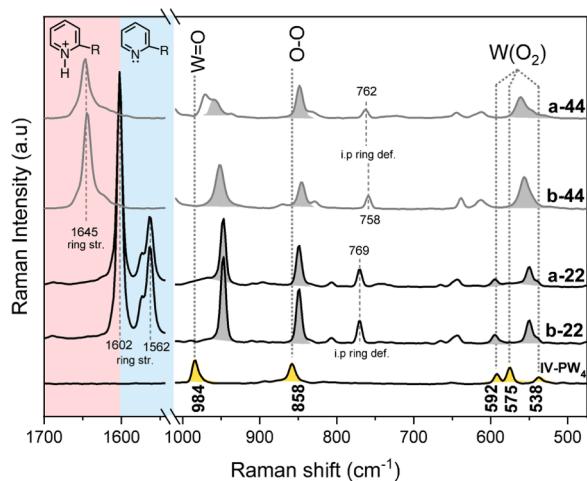


Fig. 5. Raman spectra of the four compounds and IV-PW₄ in the mid- and low-frequency regions. Abbreviations: str. stands for stretching; i.p stand for in-plane; def. stands for deformation (band assignment of ligand from [42]).

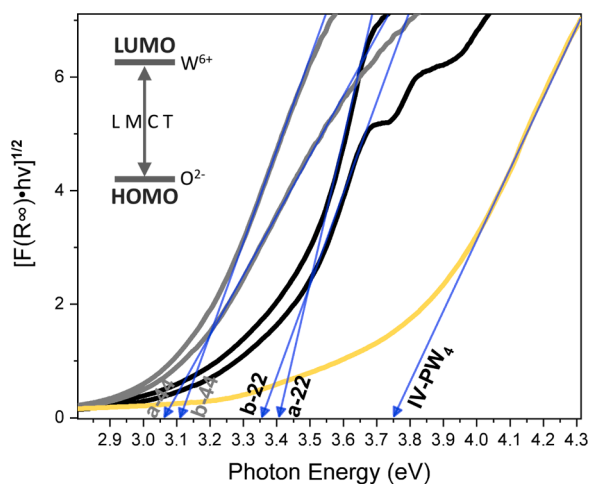


Fig. 6. Band gap (E_g) energy values determined from Tauc's relation $[F(R_{\infty}) \cdot hv]^{1/2}$ vs. photon energy for the four compounds and IV-PW₄.

washing and purification steps. The spectra of the recrystallized and as such samples show pure signals of PW₄ (Fig. S14) [67]. A plausible interpretation of these results may be given based on the dynamic equilibrium of the PW_n species (Scheme 2).

Namely, if the concentration of PW₄ in the aqueous solution decreases due to hybridization, the equilibrium that is momentarily out of balance shifts instantaneously to produce more PW₄ (at the expense of the other PW_n species) and therefore rebalances to self-compensate for the generated loss. Hence, in the Venturello system, during the dynamic interconversion of species, those that most contributed to the compensatory formation of PW₄ were PW₃ followed by PW₂, i.e., the species with the highest degree of condensation or richest tungsten content. Therefore, based on the spectroscopic data acquired from the Venturello system, the analysis of the filtrated solution B was then extended to our system. The samples showing the highest (a-22) and lowest (a-44) phosphorus contents (Table S1) and corresponding highest and lowest catalytic activities (Fig. 2) were examined. In addition, the THACl ligand was included in the hybridization process, to evaluate whether under the H₃PW₁₂O₄₀/H₂O₂/H₃PO₄ conditions, PW₄ can also be selectively precipitated (hereafter noted K-PW₄).

The spectra of the filtrated solutions (Fig. 10b–d) display all signals slightly moved downfield compared to those in solution A (Fig. 10a).

This shift is presumably due to the lower concentration of H₂O₂ in the filtrate since the opposite behavior was observed when the signal of PO₄³⁻ (without H₂O₂) was upfield-shifted in the presence of H₂O₂ (Fig. 8b).

For a better visual comparison, the integrated signals of each spectrum were grouped by type of species (inset of Fig. 10). The ligand THACl (Fig. 10d) shows to have consumed most of the PW_n species followed by 2,2'-bpy (Fig. 10b), and 4,4'-bpy (Fig. 10c). These results are also consistent with the atomic phosphorus content of each of the collected hybridized solids (Table S1).

Notice that, the relative integral decay of the PW_n species in the filtrates appears to follow the same consumption order as in the Venturello H₂WO₄/H₂O₂/H₃PO₄ system. In other words, the tungsten-rich PW_n species are the most consumed by the ligands (i.e., PW₄ > PW₃ > PW₂), while the phosphorus-rich PW_n species such as PO₄³⁻ and PW, tend to increase their concentrations due to equilibrium (except for THACl which slightly consumes PW).

³¹P NMR analysis of the solid precipitated by THACl (Fig. 10d), i.e., K-PW₄, which is fully soluble in CD₃CN/CDCl₃ (9:1) shows only the presence of PW₄ (see Fig. S15, and Table S1), confirming that THACl selectively precipitates PW₄ from the H₃PW₁₂O₄₀/H₂O₂/H₃PO₄ system. On the other hand, the ³¹P NMR spectra of precipitates a-22 and a-44, whose liquid samples were obtained by filtering the suspension formed in CD₃CN/CDCl₃ (9:1), do not display phosphorus signals (Fig. S15). Their ¹H NMR spectra, however, show resonance signals in the range of 7.3–9.5 ppm (Fig. S16). Comparison with neutral 2,2'-bpy and 4,4'-bpy ligands confirms the presence of hybridized bipyridine species dissolved in the reaction medium. The increase of proton signals in a-22 relative to neutral 2,2'-bpy, proves that 2,2'-bpy in a-22 is coordinated to a tungsten atom [68]. On the other hand, the position and number of peaks of hybridized 4,4'-bpy are similar to those of neutral 4,4'-bpy, indicating that the two pyridyl rings of hybridized 4,4'-bpy are equivalent and thus likely protonated.

Let us recall that among all compounds, a-22 has the highest phosphorus content and closest W/P (9/1) atomic ratio compared to IV-PW₄ (4/1). Since a-22 exhibits activity after hot filtration and proton signals when dissolved in CD₃CN/CDCl₃ (9:1), phosphorus signals in the ³¹P NMR spectrum are then expected. The fact that no appreciable ³¹P NMR peak was observed, indicates that only a small portion of the total phosphorus content is soluble in the reaction medium, and possibly, in a concentration where the intensity of the peak is at the level of ³¹P NMR noise signal and thus unnoticeable. Finally, based on the spectra of Fig. 10, it can be concluded that the phosphorus content detected by the elemental analysis and presumably a key player in the catalytic reaction, corresponds to phosphatooxoperoxotungstates species (PW_n) species. However, the low solubility of the hybridized phosphorus content in the employed solvents limits the possibility to exactly identify these species by means of liquid ³¹P NMR. Nevertheless, based on the selective precipitation of PW₄ by THACl in the H₃PW₁₂O₄₀/H₂O₂/H₃PO₄ and Venturello H₂WO₄/H₂O₂/H₃PO₄ systems, it can be indirectly stated that these species correspond to high-nuclearity PW_n species, predominantly PW₄ and in a lesser extent PW₃ > PW₂.

Conclusion

Isomers of bipyridine were shown to effectively form new inorganic-organic compound materials under Ishii-Venturello conditions. The external H₃PO₄ source added to the Ishii H₃PW₁₂O₄₀/H₂O₂ system triggers a structural change in compounds composed of isomer 4,4'-bpy but maintains the structure of those with 2,2'-bpy. Regardless of the H₃PO₄ addition, compounds constructed from 2,2'-bpy are substantially more active in the epoxidation than compounds containing 4,4'-bpy. Thermogravimetric and elemental analysis show that compounds of 2,2'-bpy contain more phosphorus than those with 4,4'-bpy. Compound with higher phosphorus content are found to be more active in the epoxidation reaction. DR-UV-Vis reveals that the most active catalysts

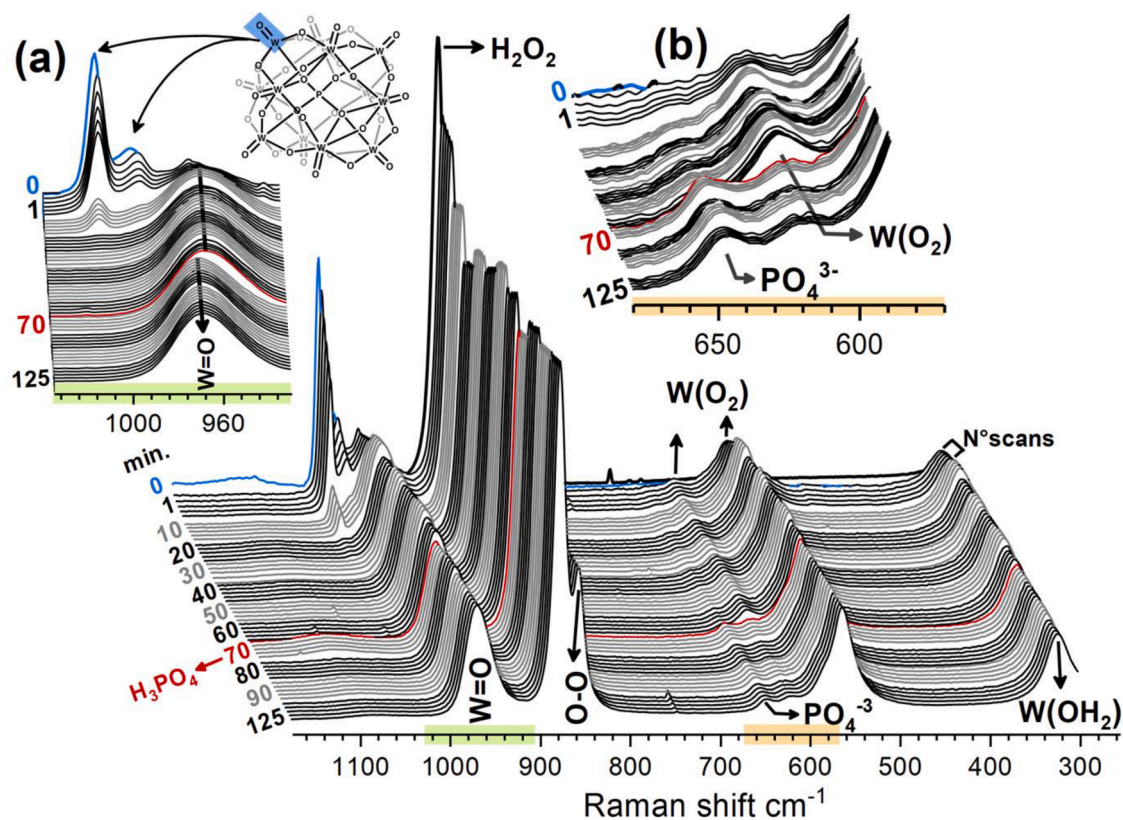


Fig. 7. Raman spectra depicting the degradation kinetics of the PW_{12} structure ($PW_{12}O_{40}^{3-}$) with H_2O_2 in solution A at room temperature. Addition of H_3PO_4 was performed after 60 min and measured at 70 min. Inset (a) depicts a zoomed view of the PW_{12} terminal $W=O$, and (b) shows the vibrational region of PO_4^{3-} . PW_{12} drawing reproduced from [64].

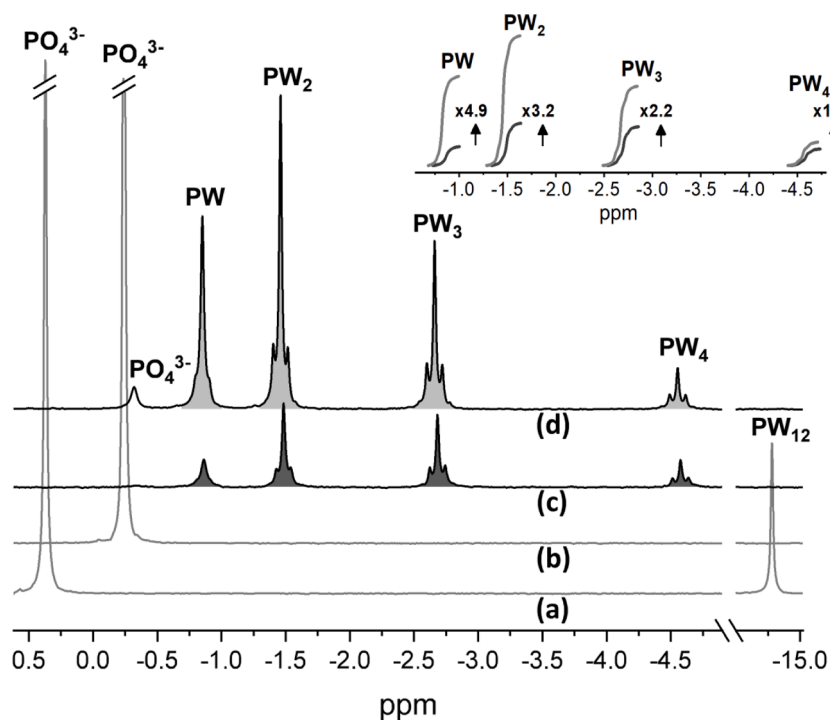


Fig. 8. ^{31}P NMR spectra (202 MHz) of: (a) $H_3PW_{12}O_{40}/H_3PO_4$ (1:2), (b) H_2O_2/H_3PO_4 (100:2), (c) $H_3PW_{12}O_{40}/H_2O_2$ (1:100), and (d) $H_3PW_{12}O_{40}/H_2O_2/H_3PO_4$ (1:100:2) aqueous systems at room temperature in 10% D_2O and 2% of trimethyl phosphate (TMP) as internal standard. The inset depicts the integrals of the PW_n species of spectra (c) and (d) with respect to TMP.

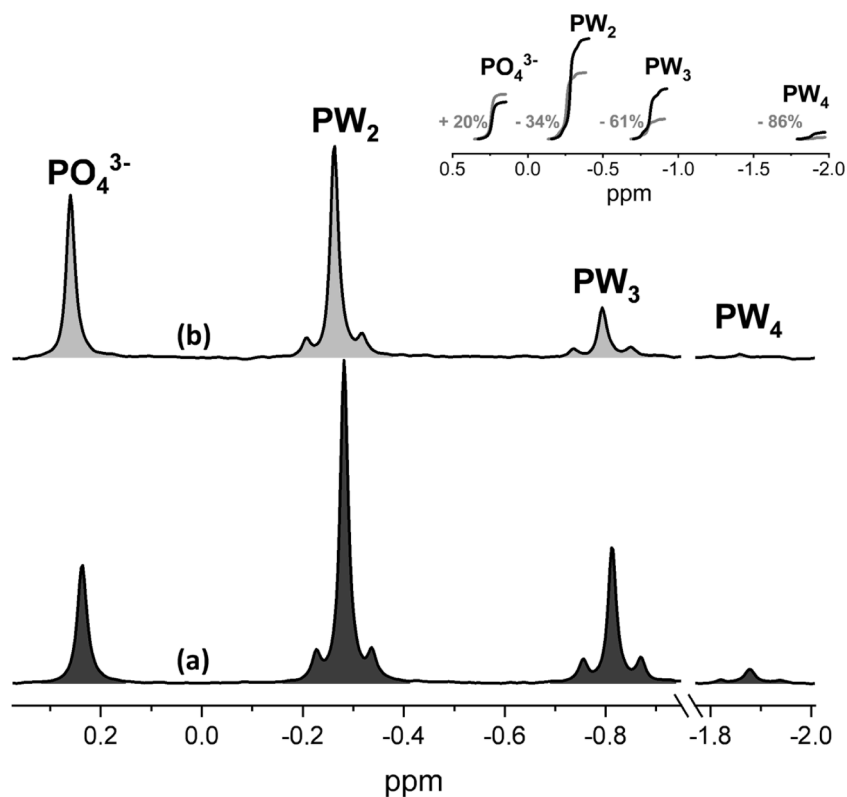


Fig. 9. ^{31}P NMR spectra (202 MHz) of: (a) $\text{H}_2\text{WO}_4/\text{H}_2\text{O}_2/\text{H}_3\text{PO}_4$ (ratios 4:28:1) and (b) refers to the filtrate of solution (a) after precipitation with THACl , in 10% D_2O and 2% TMP. The Inset plot compares the relative integration values (in percentage) of the PW_n resonant signals of each spectrum.

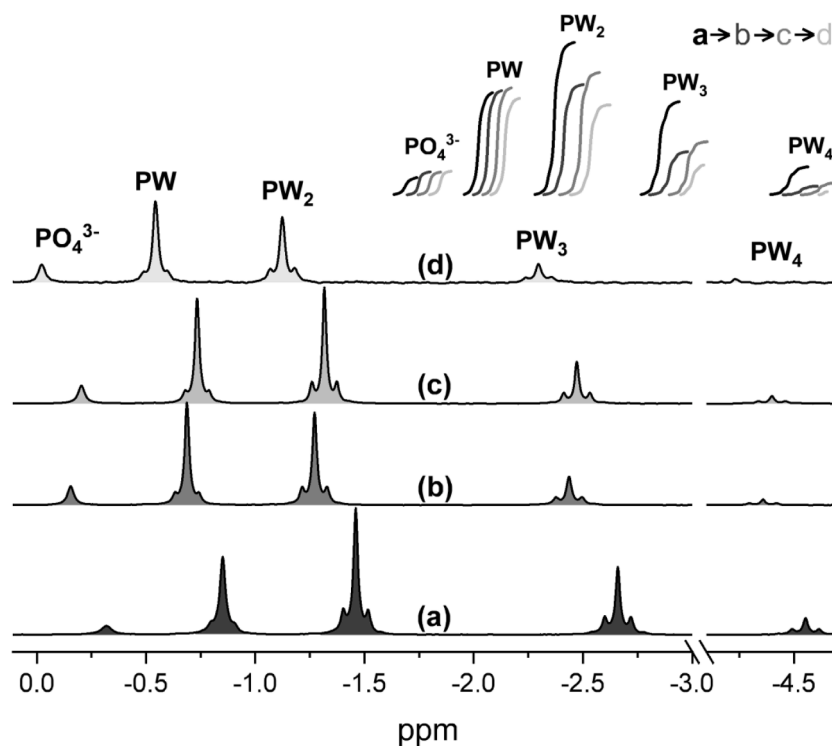


Fig. 10. ^{31}P NMR spectra (202 MHz) of: (a) $\text{H}_3\text{PW}_{12}\text{O}_{40}/\text{H}_2\text{O}_2/\text{H}_3\text{PO}_4$ (1:100:2); (b), (c), and (d) refer to the filtrate of solution (a) after addition of 2,2'-bpy, 4,4'-bpy, and THACl respectively, in 10% D_2O and 2% TMP. The inset depicts the integrated signals of PW_n species of each spectrum organized by group of species.

present the highest band gap energy and, in turn, the highest phosphorus content. Vibrational spectroscopies show that the anionic part of the compounds is composed of oxidiperoxotungstate $\text{WO}(\text{O}_2)_2$ moieties

which interact electrostatically with 4,4'-bpy and in a coordination mode with 2,2'-bpy. The benchmark IV- PW_4 , which shows the poorest catalytic activity under the employed conditions, is not effectively

reoxygenated by H₂O₂, and therefore has its initial structure damaged. On the contrary, the more active and partially soluble 2,2'-bpy-based catalysts show to epoxidize momentarily in the homogeneous phase and later precipitate as the epoxide product builds up, providing a valuable opportunity for separation and reuse. The role of H₂O₂ was demonstrated to be critical not only for inducing the epoxidation activity, but for its pivotal role as conservative agent. The absence of H₂O₂ in the reaction medium caused an irreversible damage to the catalysts structure, shedding light on its participation as a presumably key intermediate species in the reaction mechanism rather than just a simple reoxygenating agent. Further liquid ³¹P NMR and Raman analysis revealed that during the synthesis of the compounds, the PW₁₂ anion of PTA is completely degraded by H₂O₂ after 30 min and consequently, the reaction produces five phosphatooxoperoxotungstates PW_n (n = 1; 2; 3; 4) species. The PW_n species are formed prior reaction with bipyridine, and their concentration increases upon reaction with H₃PO₄. The phosphorus content initially detected, was indirectly identified by liquid ³¹P NMR as PW_n specie(s) predominantly with high n value. This was deduced from the observed dynamic interconversion of PW_n species during the selective precipitation of PW₄ with THACl under identical conditions. Finally, this study shows that bipyridine ligands, or any other related organonitrogen compound, are ideal candidates to expand the limited library of cations used in Ishii-Venturello system and, thereby, could provide more possibilities for the development of innovative type of epoxidation catalysts of increased complexity.

CRedit authorship contribution statement

Gabriel Hidalgo: Writing – original draft, Conceptualization, Methodology, Investigation, Formal analysis, Visualization. **Gabriella Barozzino-Consiglio:** Validation, Investigation, Formal analysis. **Michél Devillers:** Conceptualization, Validation, Resources, Writing – review & editing. **Eric M. Gagneaux:** Conceptualization, Supervision, Resources, Project administration, Funding acquisition, Writing – review & editing.

Declaration of Competing Interest

The authors declare that they have no known competing financial interests or personal relationships that could have appeared to influence the work reported in this paper.

Data Availability

Data will be made available on request.

Acknowledgments

Authors acknowledge the 'Communauté française de Belgique' for the financial support through the ARC programme (15/20-069) and the purchase of the equipment thanks to F.N.R.S. (projects CDR J.0156.18 for DRUV and EQP U.N006.16 for PXRD).

Supplementary materials

Supplementary material associated with this article can be found, in the online version, at doi:10.1016/j.mcat.2022.112479.

References

- S.S. Wang, G.Y. Yang, Recent advances in polyoxometalate-catalyzed reactions, *Chem. Rev.* 115 (11) (2015) 4893–4962.
- G. Strukul, G. Strukul, Catalytic oxidations with hydrogen peroxide as oxidant, in: *Catalysis by Metal Complexes*, 9, Springer, the Netherlands: Dordrecht, 1992.
- I.V. Kozhevnikov, Catalysis by heteropoly acids and multicomponent polyoxometalates in liquid-phase reactions, *Chem. Rev.* 98 (1) (1998) 171–198.
- N. Mizuno, K. Yamaguchi, K. Kamata, Epoxidation of olefins with hydrogen peroxide catalyzed by polyoxometalates, *Coord. Chem. Rev.* 249 (17–18 SPEC. ISS) (2005) 1944–1956.
- Y. Ishii, K. Yamawaki, T. Ura, H. Yamada, T. Yoshida, M. Ogawa, Hydrogen peroxide oxidation catalyzed by heteropoly acids combined with cetylpyridinium chloride. Epoxidation of olefins and allylic alcohols, ketonization of alcohols and diols, and oxidative cleavage of 1,2-diols and olefins, *J. Org. Chem.* 53 (15) (1988) 3587–3593.
- Y. Ishii, K. Yamawaki, T. Yoshida, T. Ura, M. Ogawa, Oxidation of olefins and alcohols by peroxo-molybdenum complex derived from tris(cetylpyridinium) 12-molybdophosphate and hydrogen peroxide, *J. Org. Chem.* 52 (9) (1987) 1868–1870.
- C. Venturello, R. D'Aloisio, J.C.J. Bart, M. Ricci, A new peroxotungsten heteropoly anion with special oxidizing properties: synthesis and structure of tetrahexylammonium tetra(diperoxotungsto)phosphate(3-), *J. Mol. Catal.* 32 (1) (1985) 107–110.
- C. Venturello, R. D'Aloisio, Quaternary ammonium tetrakis(diperoxotungsto) phosphates(3-) as a new class of catalysts for efficient alkene epoxidation with hydrogen peroxide, *J. Org. Chem.* 53 (7) (1988) 1553–1557.
- C. Aubry, J.M. Brégeault, G. Chottard, R. Thouvenot, N. Platzer, F. Chauveau, C. Huet, H. Ledon, Reinvestigation of epoxidation using tungsten-based precursors and hydrogen peroxide in a biphasic medium, *Inorg. Chem.* 30 (23) (1991) 4409–4415.
- A.C. Dengel, W.P. Griffith, B.C. Parkin, Studies on polyoxo- and POLYPEROXO-METALATES. Part 1. Tetrameric heteropolyperoxotungstates and heteropolyperoxomolybdates, *J. Chem. Soc. Dalton Trans.* 1 (18) (1993) 2683–2688.
- L. Salles, C. Aubry, R. Thouvenot, F. Robert, C. Dorémieux-Morin, G. Chottard, H. Ledon, Y. Jeannin, J.M. Brégeault, ³¹P and ¹⁸³W NMR spectroscopic evidence for novel peroxo species in the "H₃[PW₁₂O₄₀]·yH₂O/H₂O₂" system. Synthesis and X-ray structure of tetrabutylammonium (μ-hydrogen phosphato)bis(μ-peroxo)bis(oxoperoxotungstate) (2-): a catalyst of olefin epoxidation I, *Inorg. Chem.* 33 (5) (1994) 871–878.
- D.C. Duncan, R.C. Chambers, E. Hecht, C.L. Hill, Mechanism and dynamics in the H₃[PW₁₂O₄₀]-catalyzed selective epoxidation of terminal olefins by H₂O₂. formation, reactivity, and stability of {PO₄[WO(O)₂]₄}³⁻, *J. Am. Chem. Soc.* 117 (2) (1995) 681–691.
- J. Sun, X. Zhao, G. Sun, S. Zeb, Y. Cui, Q. You, Thermodynamic and kinetic study on the catalytic epoxidation of allyl chloride with H₂O₂ by new catalyst [(C₁₈H₃₇)₂(CH₃)₂N]₃[PO₄[W(O)(O₂)₂]₄], *Chem. Eng. J.* 398 (April) (2020), 125051.
- X. Zhao, J. Sun, G. Sun, Q. You, X. Jiang, Y. Cui, Epoxidation of allyl chloride with H₂O₂ catalyzed by three structurally related quaternary ammonium modified polyoxophosphotungstates, *Appl. Catal. A Gen.* 608 (May) (2020), 117846.
- Z.P. Pai, Y.A. Chesalov, P.V. Berdnikova, E.A. Usamin, D.Y. Yushchenko, Y. V. Uchenova, T.B. Khlebnikova, V.P. Baltakhinov, D.I. Kochubey, V.I. Bukhtiyarov, Tungsten peroxopolyoxo complexes as advanced catalysts for the oxidation of organic compounds with hydrogen peroxide, *Appl. Catal. A Gen.* 604 (April) (2020), 117786.
- Á.G. Sathicq, L.R. Pizzio, P.G. Vázquez, P. Tundo, F. Aricò, G.P. Romanelli, Keggin heteropolyacid as catalyst for olefin epoxidation: a multiphase approach, *Sustain. Chem. Pharm.* 15 (257) (2020), 100201.
- F. Schmidt, M. Cokoja, Supramolecular concepts for the biphasic epoxidation of olefins using aqueous hydrogen peroxide, *Green Chem.* 23 (2) (2021) 708–722.
- N.T. Thuy, P.N. Lan, Epoxidation of Vietnam rubber seed oil by using peroxophosphatotungstate catalyst complex based on Na₂WO₄/H₃PO₄/H₂O₂ with the presence of phase-transfer catalyst, *Mol. Catal.* 509 (May) (2021), 111645.
- Y. Gao, D. Julião, D.F. Silva, B. de Castro, J. Zhao, S.S. Balula, A simple desulfurization process to achieve high efficiency, sustainability and cost-effectivity via peroxotungstate catalyst, *Mol. Catal.* 505 (January) (2021), 111515.
- C. Swalus, B. Farin, F. Gillard, M. Devillers, E.M. Gagneaux, Hybrid peroxotungstophosphate organized catalysts highly active and selective in alkene epoxidation, *Catal. Commun.* 37 (2013) 80–84.
- S. Nojima, K. Kamata, K. Suzuki, K. Yamaguchi, N. Mizuno, Selective oxidation with aqueous hydrogen peroxide by [PO₄{WO(O)₂]₄}³⁻ supported on zinc-modified tin dioxide, *ChemCatChem* 7 (7) (2015) 1097–1104.
- V.Y. Evtushok, I.D. Ivanchikova, O.Y. Podyacheva, O.A. Stonkus, A.N. Suboch, Y. A. Chesalov, O.V. Zalomaeva, O.A. Kholdeeva, Carbon nanotubes modified by venturoello complex as highly efficient catalysts for alkene and thioethers oxidation with hydrogen peroxide, *Front. Chem.* 7 (December) (2019) 1–14.
- M. Masteri-Farahani, M.K. Alavijeh, M.S. Hosseini, Venturello anion immobilized on the surface of porous activated carbon as heterogeneous catalyst for the epoxidation of olefins, *React. Kinet. Mech. Catal.* 130 (1) (2020) 303–315.
- H. Kawashima, Y. Okuda, M. Kijima, T. Fujitani, J.C. Choi, Epoxidation of microalgal biomass-derived squalene with hydrogen peroxide using solid heterogeneous tungsten-based catalyst, *Tetrahedron* 76 (16) (2020), 131109.
- Y. Gao, F. Mirante, B. de Castro, J. Zhao, L. Cunha-Silva, S.S. Balula, An effective hybrid heterogeneous catalyst to desulfurize diesel: peroxotungstate@ metal-organic framework, *Molecules* 25 (23) (2020) 5494.
- P.J. Zapf, R.C. Haushalter, J. Zubieta, Hydrothermal synthesis and structural characterization of a series of one-dimensional organic/inorganic hybrid materials of the [(MoO₃)_n(2,2'-Bipy)_m] family: [MoO₃(2,2'-Bipy)], [Mo₂O₆(2,2'-Bipy)], and [Mo₃O₉(2,2'-Bipy)₂], *Chem. Mater.* 9 (9) (1997) 2019–2024.
- D. Hagrman, P.J. Hagrman, J. Zubieta, The structural role of metal-organonitrogen subunits in the molecular manipulation of molybdenum oxides, *Comments Inorg. Chem.* 21 (4–6) (1999) 225–261.

- [28] D. Hagrman, P. Hagrman, J. Zubieta, Polyoxomolybdate clusters and copper-organonitrogen complexes as building blocks for the construction of composite solids, *Inorg. Chim. Acta* 300–302 (2000) 212–224.
- [29] P.J. Hagrman, J. Zubieta, Structural influences of organonitrogen ligands on vanadium oxide solids. hydrothermal syntheses and structures of the terpyridine vanadates $[V_2O_4(\text{Terpy})_2]_3[V_{10}O_{28}]$, $[VO_2(\text{Terpy})][V_4O_{10}]$, and $[V_9O_{22}(\text{Terpy})_3]$, *Inorg. Chem.* 39 (15) (2000) 3252–3260.
- [30] N.N. Vlasova, Effect of 2,2'-bipyridine on the adsorption of Zn^{2+} ions onto silica surface, *J. Colloid Interface Sci.* 233 (2) (2001) 227–233.
- [31] D. Ma, Y. Li, Z. Li, Tuning the moisture stability of metal-organic frameworks by incorporating hydrophobic functional groups at different positions of ligands, *Chem. Commun.* 47 (26) (2011) 7377–7379.
- [32] Y. Liu, C. Li, W. Miao, W. Tang, D. Xue, J. Xiao, T. Zhang, C. Wang, Rhodium-terpyridine catalyzed redox-neutral depolymerization of lignin in water, *Green Chem.* 22 (1) (2020) 33–38.
- [33] Y.J. Park, K.H. Jung, K.K. Park, T.Y. Eom, Hydrophobic effects of O-phenanthroline and 2,2'-bipyridine on adsorption of metal(II) ions onto silica gel surface, *J. Colloid Interface Sci.* 160 (2) (1993) 324–331.
- [34] M. Devillers, G. Hidalgo Gutierrez, E.M. Gaigneaux, Hydrophobic hybrids constructed from kegginn phosphotungstic acid and bipyridine as heterogeneous epoxidation catalysts, in: Proceedings of the Abstracts of the 14th European Congress on Catalysis, 2019.
- [35] A. Moissette, Y. Batonneau, C. Brémard, Conformation and protonation of 2,2'-bipyridine and 4,4'-bipyridine in acidic aqueous media and acidic ZSM-5 zeolites: a raman scattering study, *J. Am. Chem. Soc.* 123 (49) (2001) 12325–12334.
- [36] C. Djordjevic, N. Vuletic, M.L. Renslo, B.C. Puryear, R. Alimard, Peroxo heteroligand vanadates(V): synthesis, spectra-structure relationships, and stability toward decomposition, *Mol. Cell. Biochem.* 153 (1–2) (1995) 25–29.
- [37] A.C. Dengel, W.P. Griffith, R.D. Powell, A.C. Skapski, Studies on transition-metal peroxo complexes. Part 7. Molybdenum(VI) and tungsten(VI) carboxylato peroxo complexes, and the X-ray crystal structure of $K_2[MoO(O_2)_2(\text{Glyc})] \cdot 2H_2O$, *J. Chem. Soc. Dalton Trans.* (5) (1987) 991–995.
- [38] N. Vuletić, C. Djordjević, Oxidoperoxovanadate(V) complexes with bidentate ligands, *J. Chem. Soc. Dalton Trans.* 2 (11) (1973) 1137.
- [39] N.J. Campbell, A.C. Dengel, C.J. Edwards, W.P. Griffith, Studies on transition metal peroxo complexes. Part 8. The nature of peroxomolybdates and peroxotungstates in aqueous solution, *J. Chem. Soc. Dalton Trans.* (6) (1989) 1203–1208, <https://doi.org/10.1039/dt9890001203>. No.
- [40] D. Cook, Vibrational spectra of pyridinium salts, *Can. J. Chem.* 39 (10) (1961) 2009–2024.
- [41] T. Lu, T.M. Cotton, R.L. Birke, J.R. Lombardi, Raman and surface-enhanced raman spectroscopy of the three redox forms of 4,4'-bipyridine, *Langmuir* 5 (3) (1989) 886, 886.
- [42] A.L. Kamyshny, V.N. Zakharov, Y.V. Fedorov, A.E. Galashin, L.A. Aslanov, Surface-enhanced raman scattering of 2,2'-bipyridine adsorbed on colloidal silver and stabilized AgBr sols, *J. Colloid Interface Sci.* 158 (1) (1993) 171–182.
- [43] T. Amarante, F. Almeida Paz, S. Gago, I. Gonçalves, M. Pillinger, A. Rodrigues, M. Abrantes, Microwave-assisted synthesis and crystal structure of oxo(diperoxo) (4,4'-di-tert-butyl-2,2'-bipyridine)-molybdenum(VI), *Molecules* 14 (9) (2009) 3610–3620.
- [44] T.R. Amarante, P. Neves, A.C. Gomes, M.M. Nolasco, P. Ribeiro-Claro, A.C. Coelho, A.A. Valente, F.A.A. Paz, S. Smeets, L.B. McCusker, M. Pillinger, I.S. Gonçalves, Synthesis, structural elucidation, and catalytic properties in olefin epoxidation of the polymeric hybrid material $[Mo_3O_9(2-[3(5)\text{-pyrazolyl}]pyridine)]_n$, *Inorg. Chem.* 53 (5) (2014) 2652–2665.
- [45] T. Okuhara, N. Mizuno, M. Misono, Catalytic chemistry of heteropoly compounds, *Adv. Catal.* 41 (C) (1996) 113–252.
- [46] C. Rocchiccioli-Deltcheff, R. Thouvenot, R. Franck, Spectres i.r. et Raman d'hétéropolyanions $\alpha\text{-XM}_{12}\text{O}_{40}^-$ de structure de type Keggin (X = B^{III} , Si^{IV} , Ge^{IV} , P^V , As^V et M = W^{VI} et Mo^{VI}), *Spectrochim. Acta Part A Mol. Spectrosc.* 32 (3) (1976) 587–597.
- [47] S.A. Bagshaw, R.P. Cooney, FTIR and Raman spectroscopic investigation of 2,2'-bipyridine adsorption on silica, alumina, zirconia and titania, *J. Mater. Chem.* 4 (4) (1994) 557–563.
- [48] D.A. Thornton, G.M. Watkins, The infrared spectra ($4000 - 50 \text{ cm}^{-1}$) of complexes of quinoline N-oxide and its perdeuterated analogue with metal(II) perchlorates of the first transition series, *J. Coord. Chem.* 29 (1–2) (1993) 45–56.
- [49] D. Masure, Polyoxometallates as models for oxide catalysts part II. Theoretical semi-empirical approach to the influence of the inner and outer Mo coordination spheres on the electronic levels of polyoxomolybdates, *J. Catal.* 119 (2) (1989) 415–425.
- [50] M. Fournier, C. Louis, M. Che, P. Chaquin, D. Masure, Polyoxometallates as models for oxide catalysts. Part I. An UV-visible reflectance study of polyoxomolybdates: influence of polyhedra arrangement on the electronic transitions and comparison with supported molybdenum catalysts, *J. Catal.* 119 (2) (1989) 400–414.
- [51] K. Nomiya, Y. Sugie, K. Amimoto, M. Miwa, Charge-transfer absorption spectra of some tungsten(VI) and molybdenum(VI) polyoxoanions, *Polyhedron* 6 (3) (1987) 519–524.
- [52] M.H. Youn, H. Kim, J.C. Jung, I.K. Song, K.P. Barteau, M.A. Barteau, UV-vis spectroscopy studies of $H_3PMo_{12-x}W_xO_{40}$ heteropolyacid (HPA) catalysts in the solid state: effects of water content and polyatom substitution, *J. Mol. Catal. A Chem.* 241 (1–2) (2005) 227–232.
- [53] V. Sasca, A. Popa, Band-gap energy of heteropoly compounds containing Keggin polyanion- $[PV_xMo_{12-x}O_{40}]^{-(3+x)}$ relates to counter-cations and temperature studied by UV-vis diffuse reflectance spectroscopy, *J. Appl. Phys.* 114 (13) (2013), 133503.
- [54] R.S. Weber, Effect of local structure on the UV-Visible absorption edges of molybdenum oxide clusters and supported molybdenum oxides, *J. Catal.* 151 (2) (1995) 470–474.
- [55] H. Mimoun, I. Sere de Roch, L. Sajus, Epoxydation des olefines par les complexes peroxydiques covalents Du MOLYBDENE—VI, *Tetrahedron* 26 (1) (1970) 37–50.
- [56] H. Mimoun, The role of peroxymetallation in selective oxidative processes, *J. Mol. Catal.* 7 (1) (1980) 1–29.
- [57] L.I. Simándi, Catalytic oxidations with hydrogen peroxide, *React. Kinet. Catal. Lett.* 50 (1–2) (1993) 423–425.
- [58] K.B. Sharpless, J.M. Townsend, D.R. Williams, Mechanism of epoxidation of olefins by covalent peroxides of molybdenum(VI), *J. Am. Chem. Soc.* 94 (1) (1972) 295–296.
- [59] D.V. Deubel, J. Sundermeyer, G. Frenking, Mechanism of the olefin epoxidation catalyzed by molybdenum diperoxo complexes: quantum-chemical calculations give an answer to a long-standing question, *J. Am. Chem. Soc.* 122 (41) (2000) 10101–10108.
- [60] W.R. Thiel, Metal Catalyzed oxidations. Part 5. Catalytic olefin epoxidation with seven-coordinate oxobisperoxo molybdenum complexes: a mechanistic study, *J. Mol. Catal. A Chem.* 117 (1–3) (1997) 449–454.
- [61] W.R. Thiel, M. Barz, H. Glas, A.K. Pleier, ChemInform abstract: olefin epoxidation catalyzed by molybdenum peroxo complexes: a mechanistic study, *Peroxide Chem.* (2000) 433–453, <https://doi.org/10.1002/3527600396.ch20>.
- [62] T. Cousin, G. Chatel, B. Andrioletti, M. Draye, Oxidative cleavage of cycloalkenes using hydrogen peroxide and a tungsten-based catalyst: towards a complete mechanistic investigation, *New J. Chem.* 45 (1) (2021) 235–242.
- [63] C. Rocchiccioli-Deltcheff, M. Fournier, R. Franck, R. Thouvenot, Vibrational Investigations of polyoxometalates. 2. evidence for anion-anion interactions in molybdenum(vi) and tungsten(vi) compounds related to the Keggin structure, *Inorg. Chem.* 22 (2) (1983) 207–216.
- [64] G.M. Brown, M.R. Noe-Spirllet, W.R. Busing, H.A. Levy, Dodecatungstophosphoric acid hexahydrate, $(H_5O_2)_3(PW_{12}O_{40})$. The true structure of Keggin's 'pentahydrate' from single-crystal X-ray and neutron diffraction data, *Acta Crystallogr. Sect. B Struct. Crystallogr. Cryst. Chem.* 33 (4) (1977) 1038–1046.
- [65] L. Salles, R. Thouvenot, J.M. Brégeault, Redistribution and fluxionality in heteropolyoxoperoxo complexes: $[PO_4(M_2O_2(\mu-O_2)_2(O_2)_2)]^{3-}$ with M = Mo and/or W, *J. Chem. Soc. Dalton Trans.* 4 (6) (2004) 904–907.
- [66] J.M. Brégeault, Transition-metal complexes for liquid-phase catalytic oxidation: some aspects of industrial reactions and of emerging technologies, *J. Chem. Soc. Dalton Trans.* 3 (17) (2003) 3289–3302.
- [67] Y. Mahha, L. Salles, J.Y. Piquemal, E. Briot, A. Atlamsani, J.M. Brégeault, Environmentally friendly epoxidation of olefins under phase-transfer catalysis conditions with hydrogen peroxide, *J. Catal.* 249 (2) (2007) 338–348.
- [68] P.K. Baker, P.L. Veale, 4,4'-bipyridine complexes of molybdenum(II) and tungsten(II), *Transit. Met. Chem.* 28 (4) (2003) 418–424.